Supporting Information

Substrate-Free Growth of N-Doped Bamboo Tube Morphology on CoNi Alloy Nanoparticles as an Electrocatalyst for Anion Exchange Membrane Fuel Cells

Anil Kumar U.,[a,b] and Vishal M. Dhavale* [a,b]

[a] CSIR-Central Electrochemical Research Institute-Madras Unit, CSIR Madras Complex, Taramani, Chennai 600113, India.

[b] Academy of Scientific and Innovative Research (AcSIR), Ghaziabad- 201 002, India.

Table of contents:

Fig. No.	Content	Page No.
	Structural Characterization	03
Fig. S1	Fe-SEM micrographs of Co-MOF and HR-TEM micrograph of Co@NC	04
Fig. S2	Fe-SEM micrograph of CoNi-MOF	04
Fig. S3	HAADF-STEM and Elemental mapping of CoNi@NC-T	05
Fig. S4	Fe-SEM micrograph of Ni@NC-T	05
Fig. S5	Fe-SEM micrograph of CoNi@NC-31 and CoNi@NC-13 and elemental mapping	06
Fig. S6	Fe-SEM micrograph of CoNi@NC-550 and CoNi@NC-750	06
Fig. S7	Comparative TG-DSC profiles	07
Fig. S8	HAADF-STEM and EDAX mapping	07
Table S1	ICP-OES sample analysis of prepared catalysts	08
Fig. S9	Comparative Raman analysis, BET and pore size distribution	08
Table S2	Comparative I_d/I_g ratios, BET surface area and Pore size distribution of CoNi@NC-T, Co@NC and Ni@NC-T	09
Fig. S10	XPS analysis of CoNi@NC-T	09
Fig. S11	Calibration of reference electrode	10
Fig. S12	Comparative cyclic voltammogram and linear sweep voltammetry of CoNi@NC-T	11
Fig. S13	Capacitive current cyclic voltammogram and corresponding anodic and cathodic slopes	12
Fig. S14	ORR curves recorded at different rotation speed of working electrode	12
Fig. S15	Koutecky-Levich (K-L) plots	13
Fig. S16	Calculation of number of electrons	13
Fig. S17	Rotating ring disk electrode study	14
Fig. S18	Stability test of Co@NC	14

Fig. S19	The comparative bar graph of electrochemical properties of the prepared catalysts	15
Fig. S20	Fe-SEM micrograph, Elemental mapping and p-XRD patterns after the stability test	16
Fig. S21	Schematic procedure of electrode fabrication and membrane electrode assembly (MEA)	16
Table S3	Electrochemical properties compared with literature reports	17-18
Table S4	AEMFC performance comparison with literature reports of various types of membranes	18-19
Table S5	AEMFC performance with Fumion based membranes	19-20

Structural characterization:

A well-dispersed sample for the high-resolution transmission electron microscope (HR-TEM) analysis was prepared by sonicating the prepared catalyst (1 mg) in 5 ml isopropanol solvent. The homogenously dispersed sample was drop-coated on a lacey carbon-coated copper grid and was dried under a vacuum. In FEI, Talos F200s instrument operated at an accelerated voltage of 200 kV transmission electron microscopy. Surface area analysis of the prepared catalysts was characterized using N_2 adsorption-desorption isotherms, measured at 77 K using Quantachrome Autosorb iQ-MP/iQ-XR. Surface area and pore sizes were determined using the Brunauer–Emmett–Teller (BET) equation, and pore size distribution (PSD) curves were obtained by the NLDFT method. Field emission scanning electron microscopic (Fe-SEM) images were recorded using a TESCAN MIRA3 LM instrument, and Gemini ZESIS SUPRA™ 55VP were used to micrograph the morphology of the prepared catalysts and SEM-EDAX analysis by 20 mm^2 X-Max from Oxford instruments. Cobalt and Nickel ratios was determined by Inductively Coupled Plasma-Mass Spectroscopy (ICP-MS) with Agilent technologies, 7700 series system. For ICP-MS analysis, the samples for are prepared by dissolving the catalyst in of aqua regia and kept for sample digestion. An transparent solution indicates the digestion of the sample, and later, it was carefully filtered using vacuum filtration and diluted by adding deionized water in standard volumetric flask. Powder X-ray diffraction (p-XRD) patterns were recorded on Bruker, D8 Advance model, having X-ray source CuKα with λ=1.5406 Å and Lynx Eye & Scintillation Counter as a detector in the 2θ range of 10–80° in 20 minutes. The induced defects, like graphitic and defective nature of the carbon surface of the surface, were understood by measuring the Raman spectrum in the range of 400 to 4000 cm^{-1} using laser raman spectroscopy technique with 532 Oxxius laser in the Horiba Jobin made LabRAM HR evolution model. X-ray photoelectron spectroscopy (XPS) measurements were carried out on a Thermo-scientific made ESCALAB 250xi BASE SYSTEM with UPS and XPS IMAGE mapping model. The thermal stability of the samples was measured and analysed using NETZSCH, STA 449 F3 model and its proteus software in both N_2 and air atmosphere with 5 °C/min.

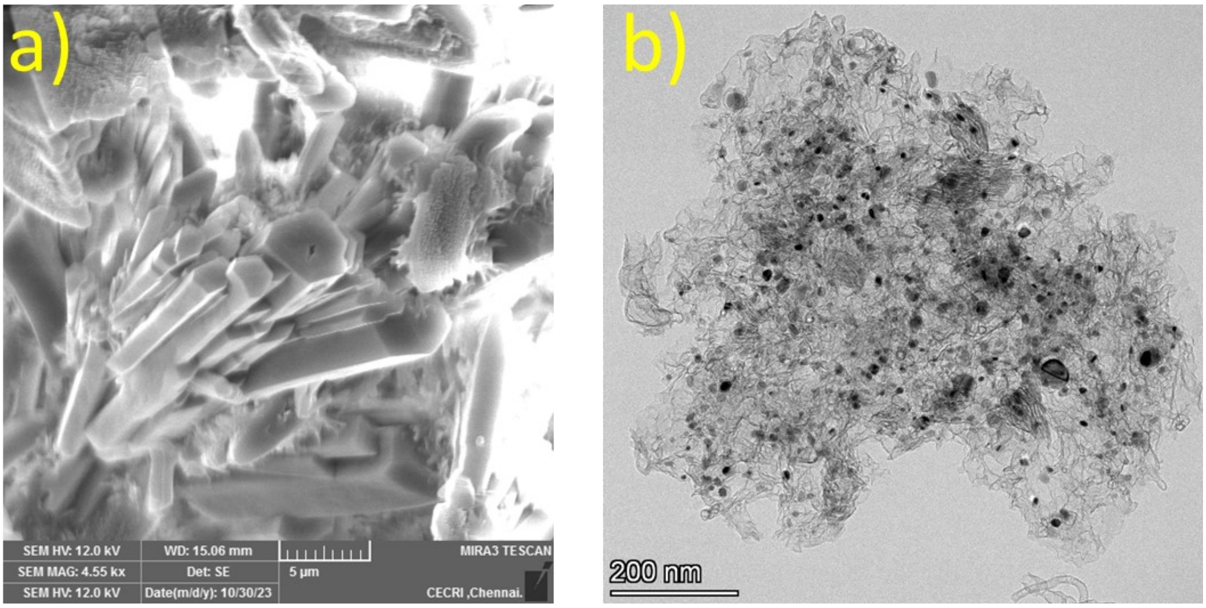

Fig. S1: (a) Fe-SEM micrograph of Co-MOF with a long hexagonal rod-like shape, (b) HR-TEM micrograph of Co@NC (Co-MOF annealed at 900 °C) showing predominant core-shell morphology with cobalt core wrapped with a N-doped carbon shell structure.

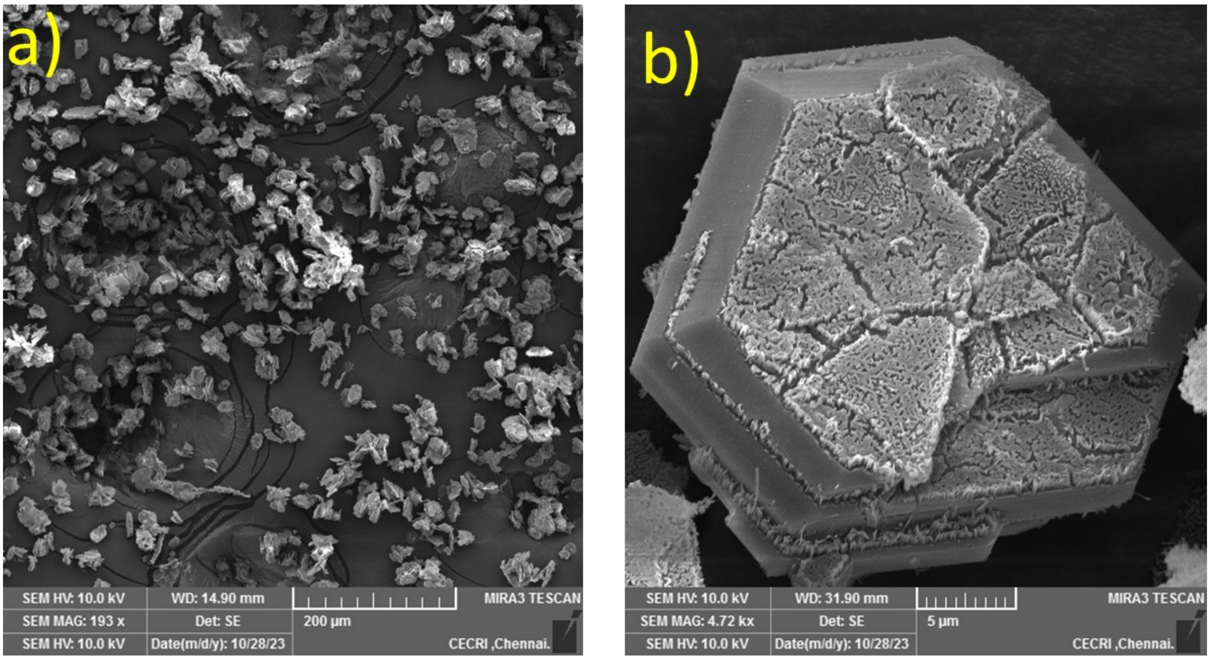

Fig. S2: (a, b) Fe-SEM micrographs of CoNi-MOF with irregular hexagon shape particles at different magnifications.

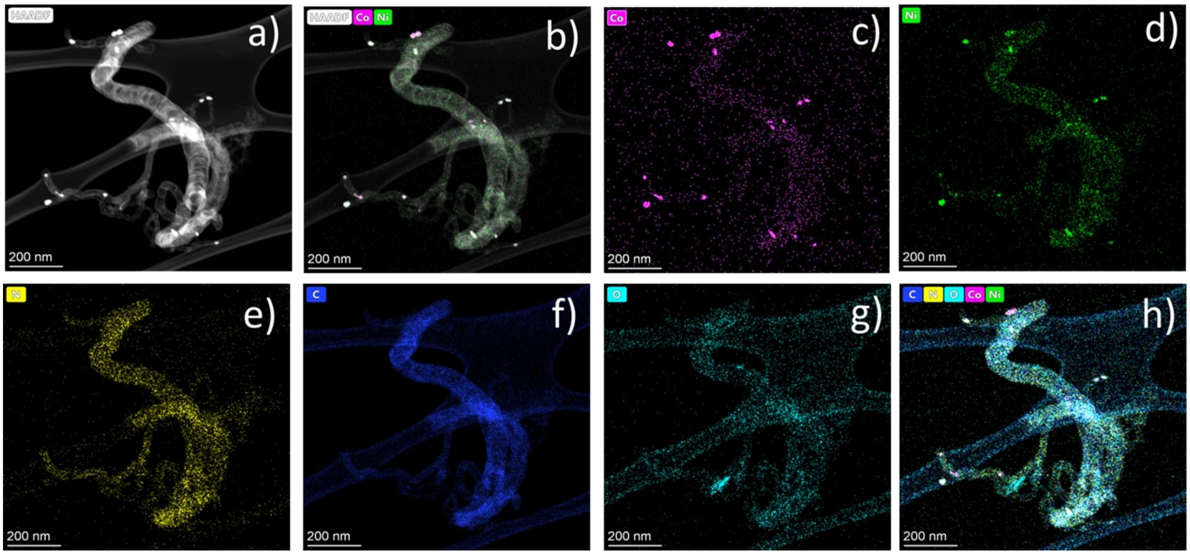

Fig. S3: (a) High angle annular dark-field (HAADF) and scanning transmission electron microscopy (STEM) images of the knotted bamboo tube-like morphology, (b) HAADF with the distribution of Co, Ni atoms along the tube and on the N-doped carbon support (c-g) Co, Ni, N, C, and O elemental mapping, respectively, and (h) combined elemental mapping of CoNi@NC-T.

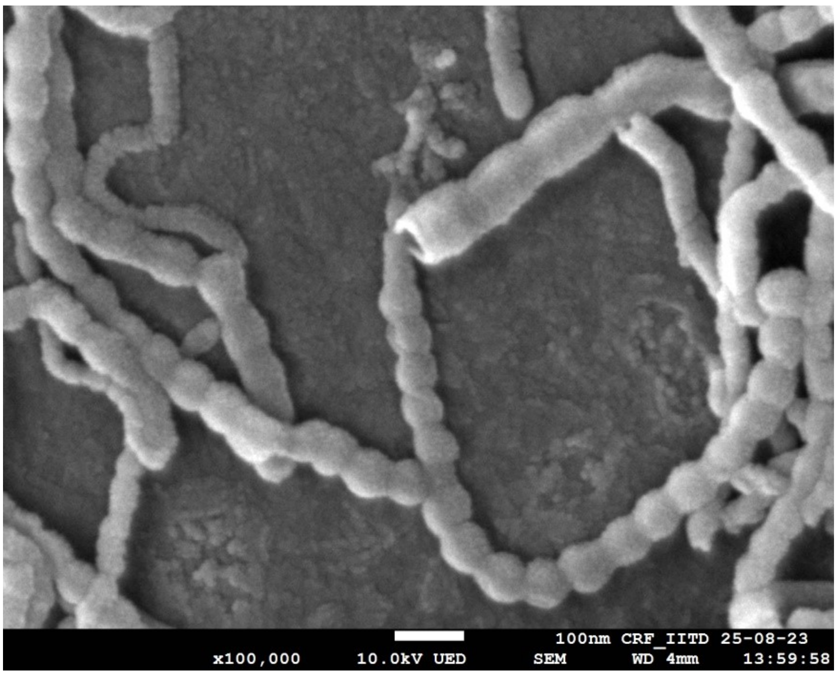

Fig. S4: Fe-SEM micrographs of Ni@NC-T (i.e., Ni-MOF annealed at 900 °C) with CNT-Necklace like structure.

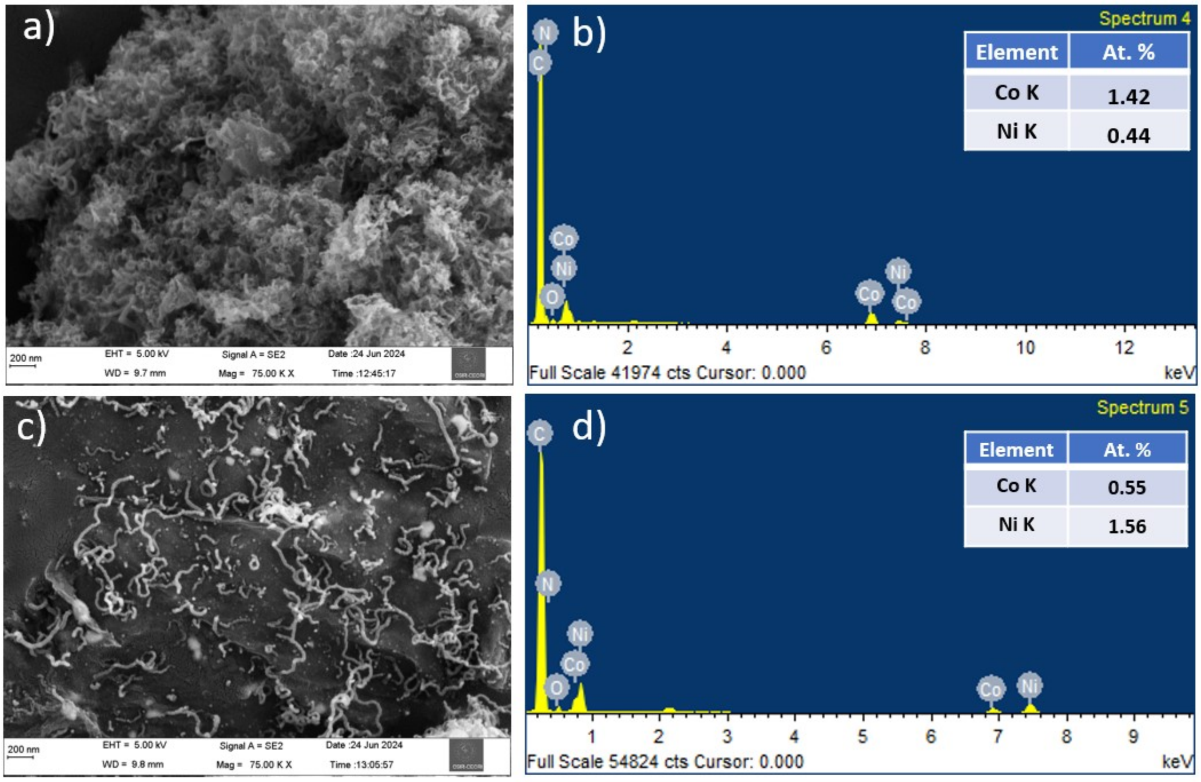

Fig. S5: Fe-SEM micrographs of (a, c) CoNi@NC-31 and CoNi@NC-13, respectively and Elemental distribution of (b, d) CoNi@NC-31 and CoNi@NC-13, respectively.

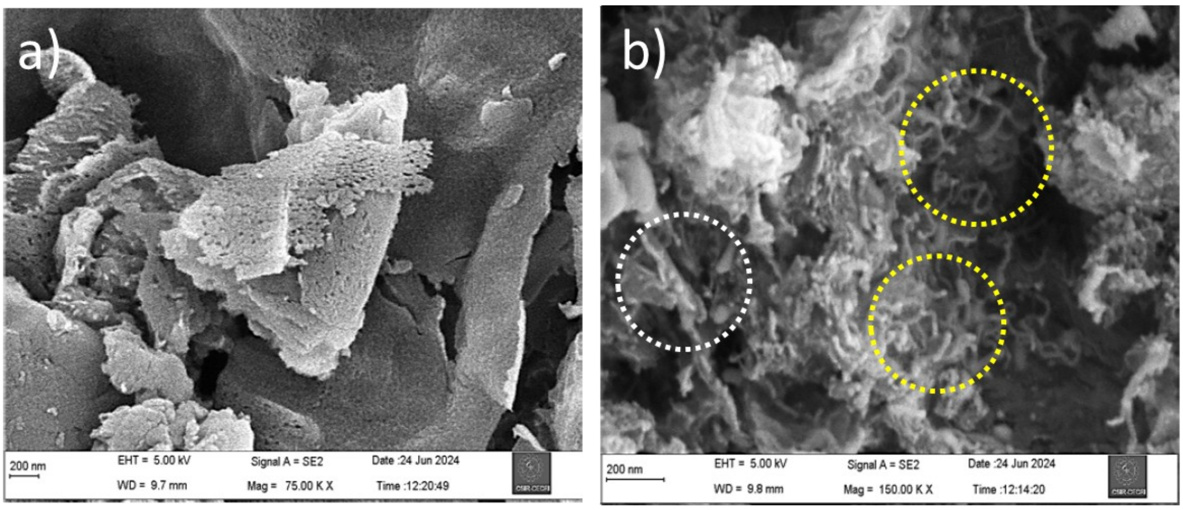

Fig. S6: (a-b) Fe-SEM micrographs of CoNi@NC-550 and CoNi@NC-750 (white circle shows sheet-like structures and yellow circles shows the formation of tubes), respectively.

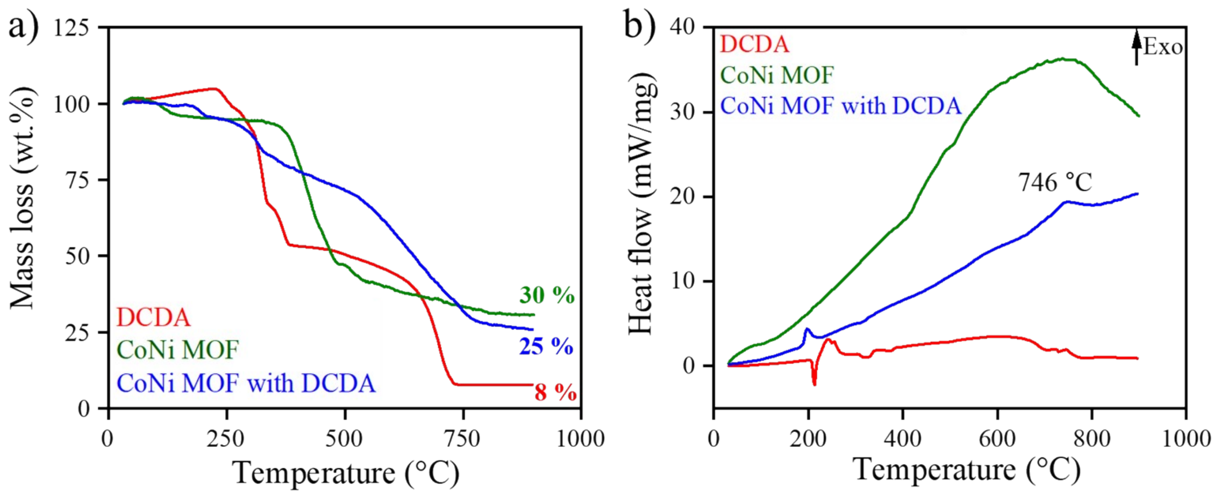

Fig. S7: (a, b) Comparative TG-DSC profiles of Dicyandiamide (DCDA), CoNi-MOF, and CoNi-MOF with DCDA samples. Data recorded in a nitrogen atmosphere.

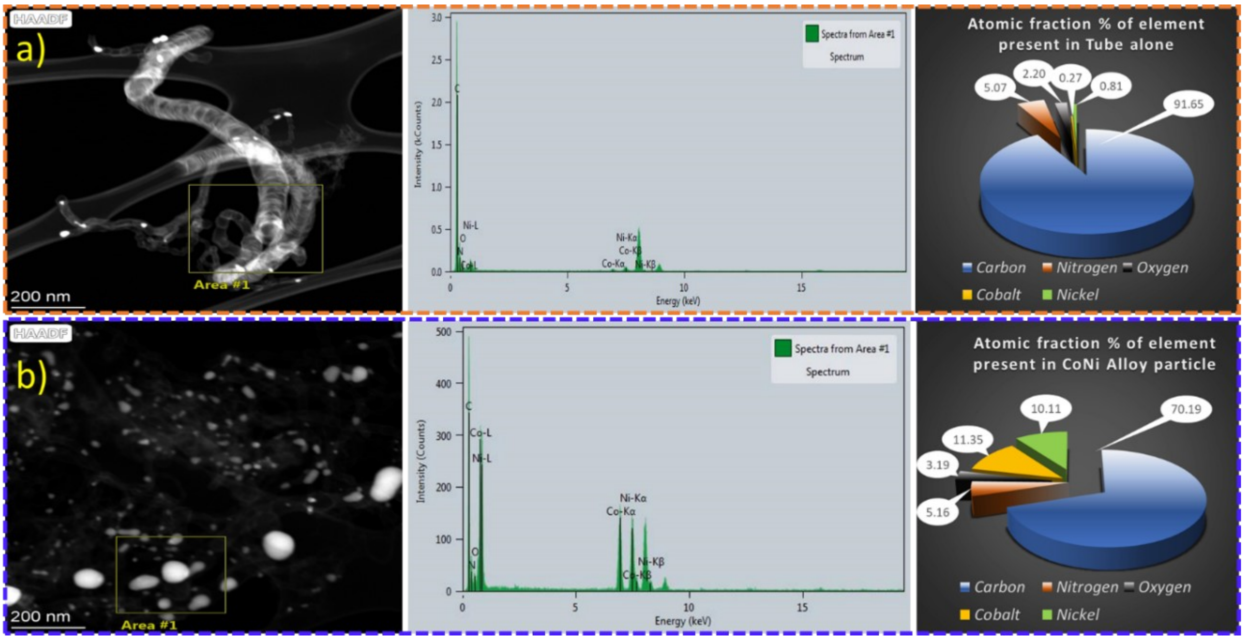

Fig. S8: High-angle annular dark-field (HAADF), EDAX spectrum, and at. % of elements, (a) on the tube, and (b) CoNi-alloy particles. [the scanned area is highlighted with a yellow-coloured square mark]

S.No.	Prepared samples	Sample code	ICP-MS Analysis (Co:Ni)
1	Co_1Ni_1	CoNi@NC-T	0.9:1.1
2	Co_1Ni_3	CoNi@NC-13	1:2.9
3	Co_3Ni_1	CoNi@NC-31	2.86:0.97

Table S1: Cobalt and Nickel ratios of the prepared catalyst measured using ICP-MS analysis.

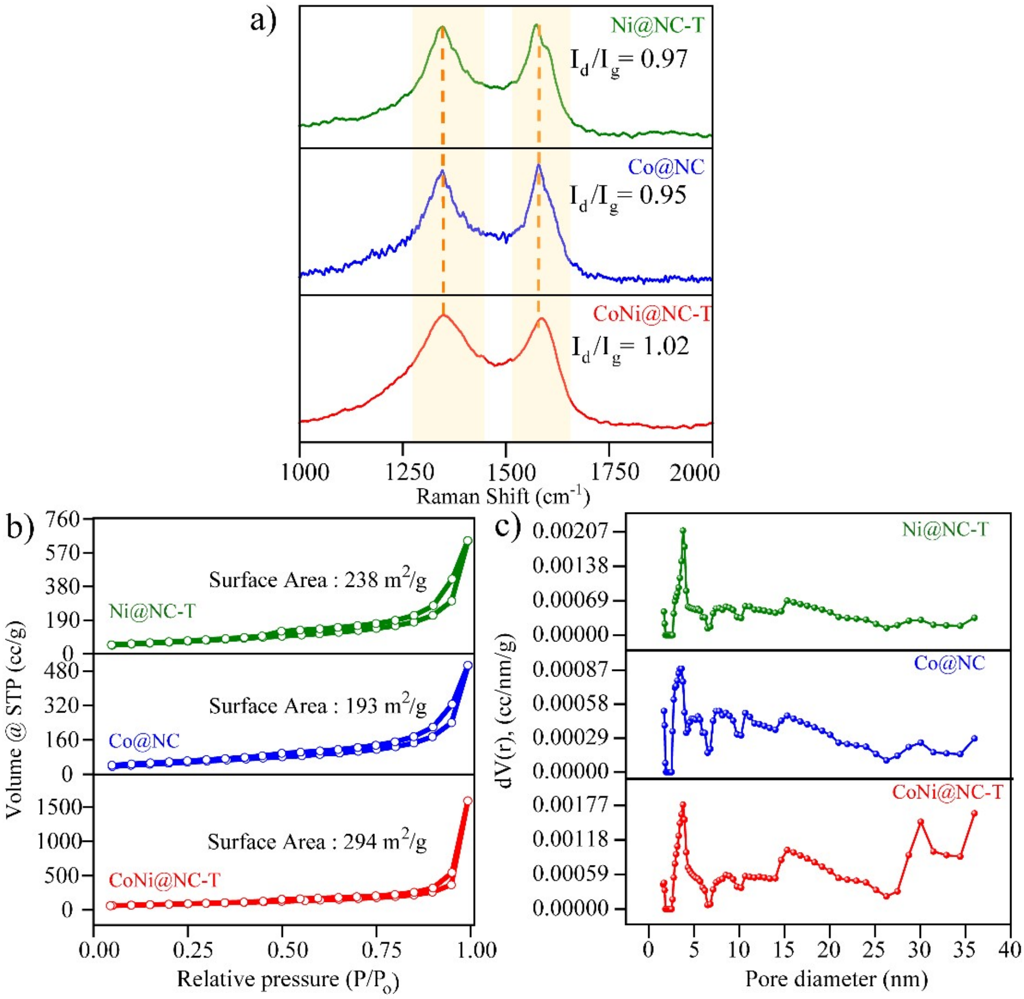

Fig. S9: (a) Comparative Raman spectra, and (b-c) Comparative BET-isotherm and Pore-size distribution of CoNi@NC-T, Co@NC, and Ni@NC-T.

Table S2: Comparative Raman and BET results for CoNi@NC-T, Ni@NC-T and Co@NC, respectively.

S.No.	Name of Catalyst	Raman Analysis	BET Analysis	
		I_d/I_g ratio	BET Surface Area (m^2/g)	Pore Volume (cc/g)
1	CoNi@NC-T	1.02	294	2.402
2	Ni@NC-T	0.97	238	0.941
3	Co@NC	0.95	193	0.745

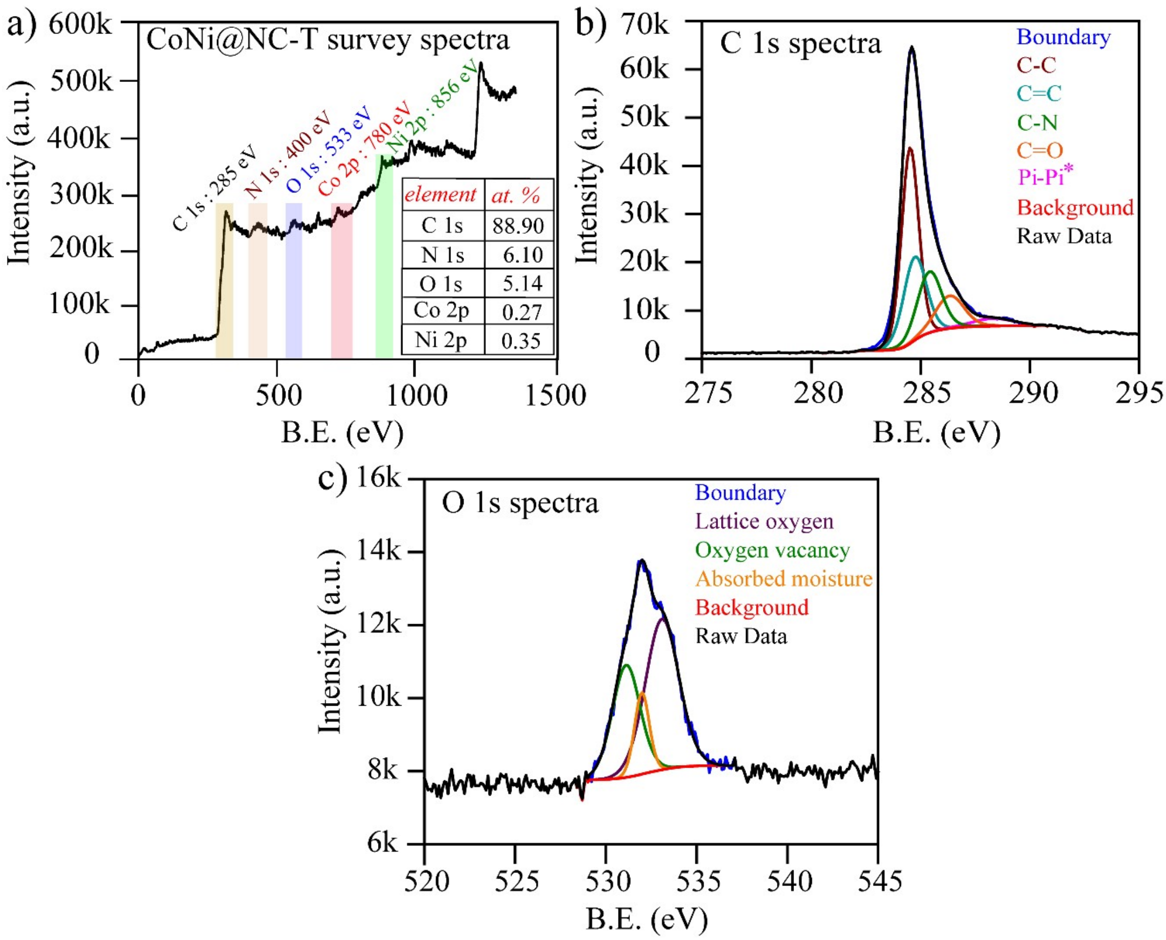

Fig. S10: XPS analysis of CoNi@NC-T, (a) survey scan, (b) C 1s spectra, and (c) O 1s spectra.

Calibration of the Hg/HgO reference electrode:

In order to convert the obtained potentials from Hg/HgO to a reversible hydrogen electrode (RHE), a LSV at a scan rate of 5 mV/s was carried out in a hydrogen-saturated 0.1 M KOH solution.

Conditions: Platinum and graphite rod were used as a working and counter electrode. The correction factor was chosen as the point at which the current crosses the zero line.

$$E_{(RHE)} = E_{(Hg/HgO)} + 0.9344 \text{ V}$$

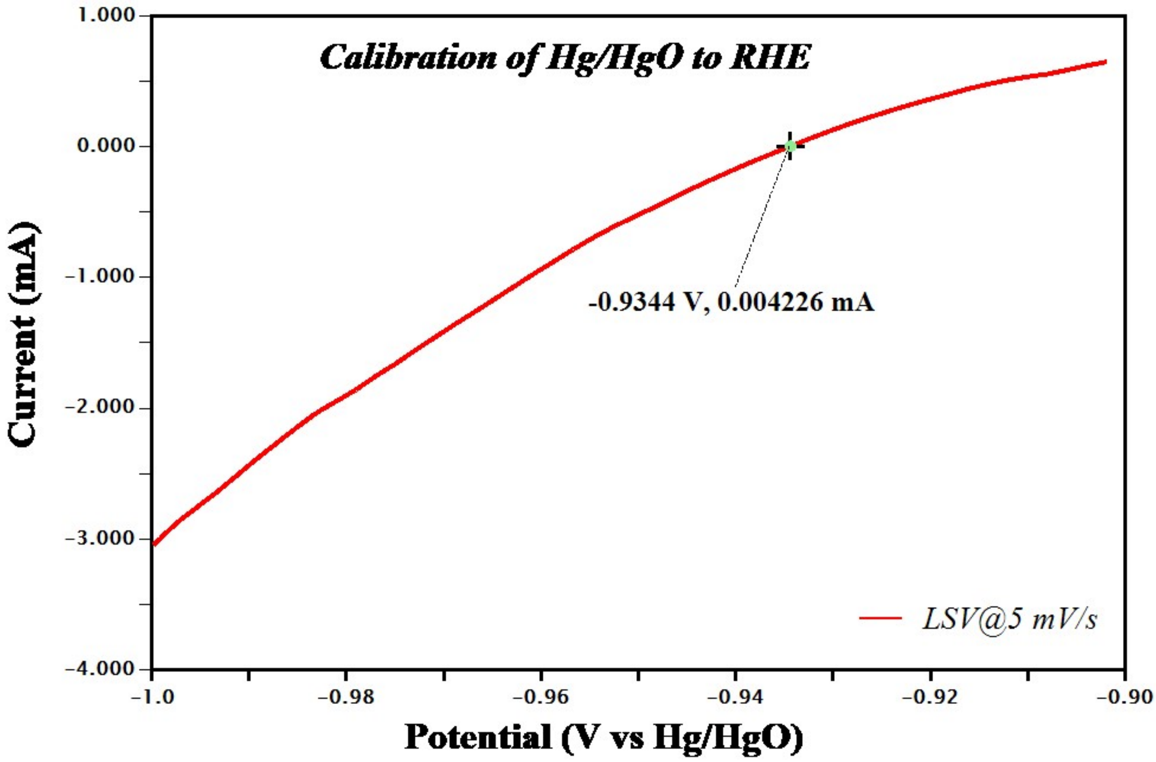

Fig. S11: Calibration LSV curve for the Hg/HgO reference electrode. (Screenshot from Aftermath software, an original data)

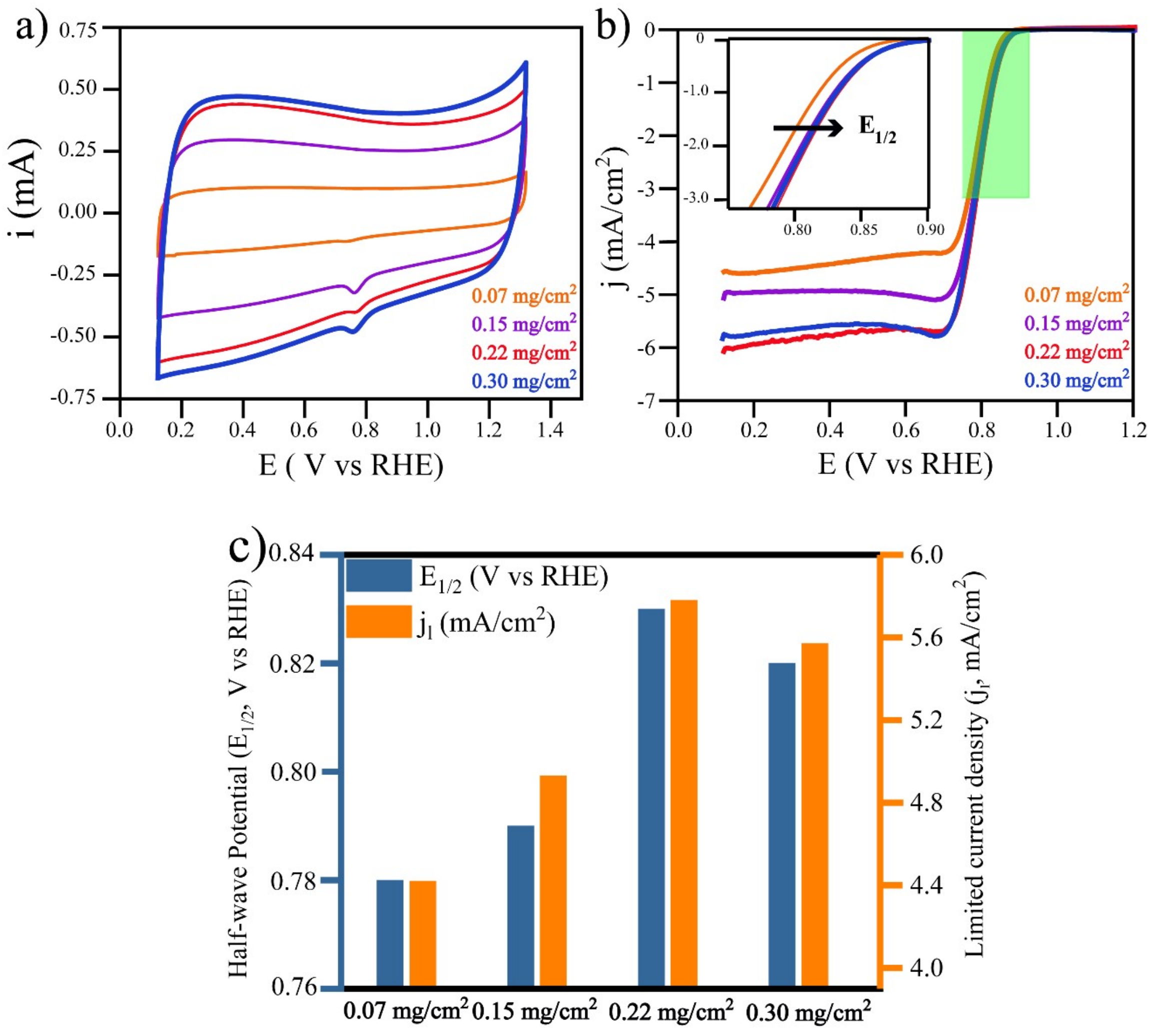

Fig. S12: (a) Cyclic voltammogram, (b) hydrodynamic LSV, and (c) change in $E_{1/2}$ (V vs RHE) and limiting current density (j_l, mA/cm^2) for various mass loading of CoNi@NC-T. Conditions: 1600 RPM, 5 mV/s scan rate, Electrolyte: oxygen saturated 0.1 M KOH solution.

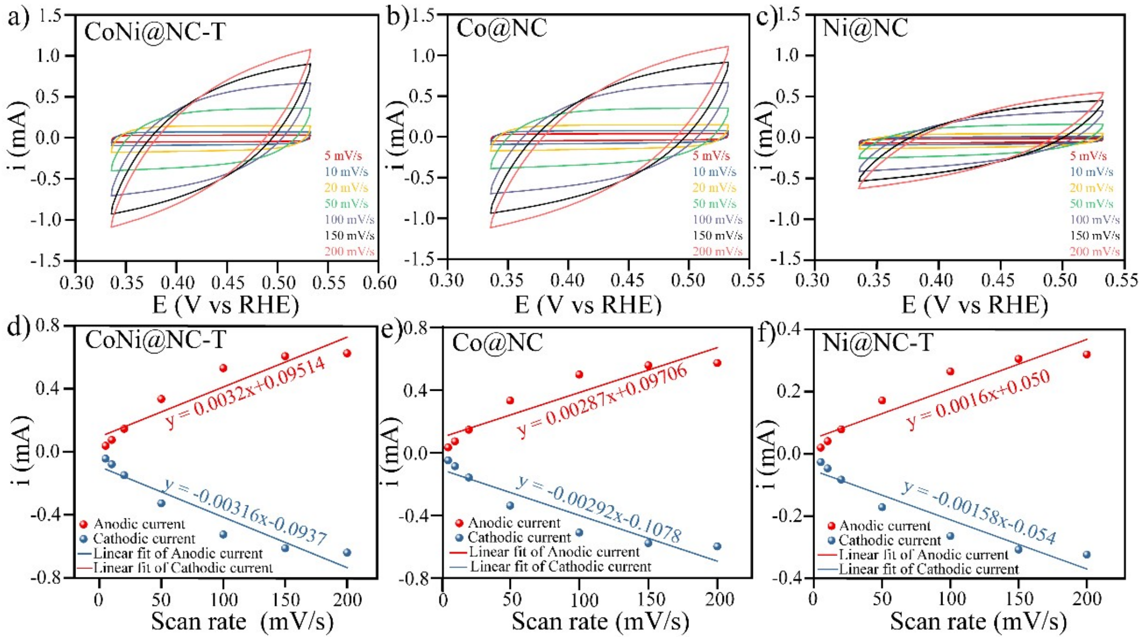

Fig. S13: (a-c) Capacitive current recorded in a nitrogen-saturated 0.1 M KOH solution with different scan rates in a potential window of 0.32 to 0.52 V, and (d-f) current vs scan rate plot at 0.42 V.

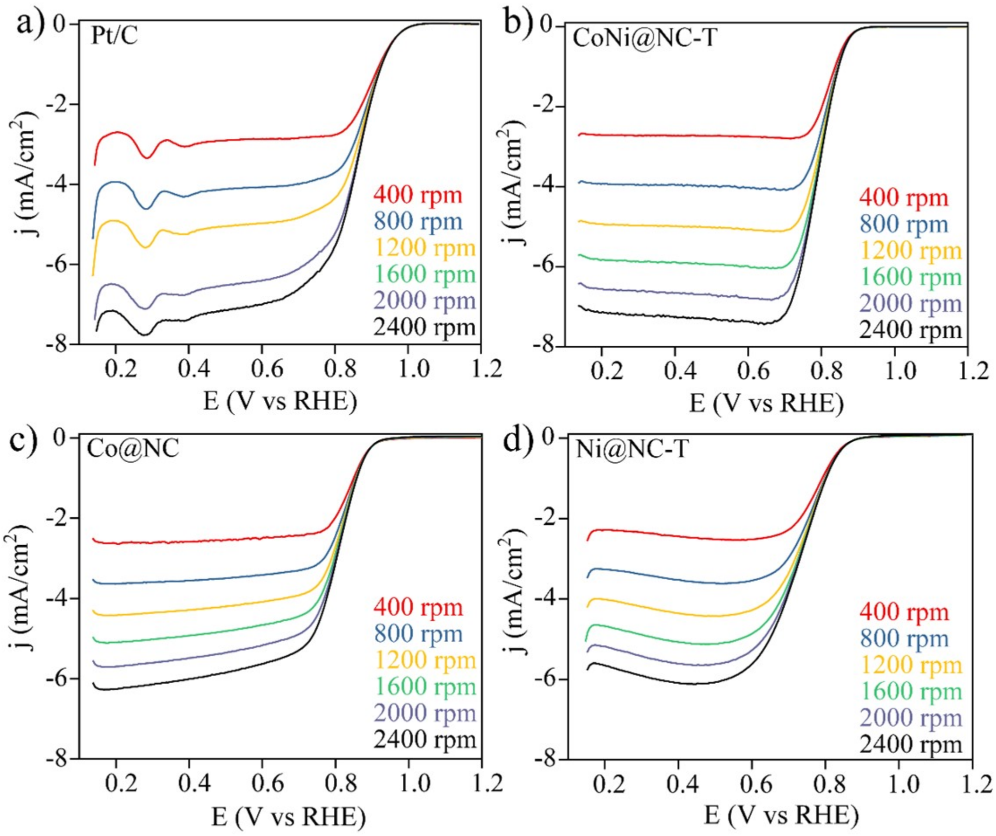

Fig. S14: (a-d) Hydrodynamic ORR curves recorded at different rotation speed of working electrode in an oxygen-saturated 0.1 M KOH solution with scan rate of 5 mV/s for Pt/C, CoNi@NC-T, Co@NC and Ni@NC-T, respectively.

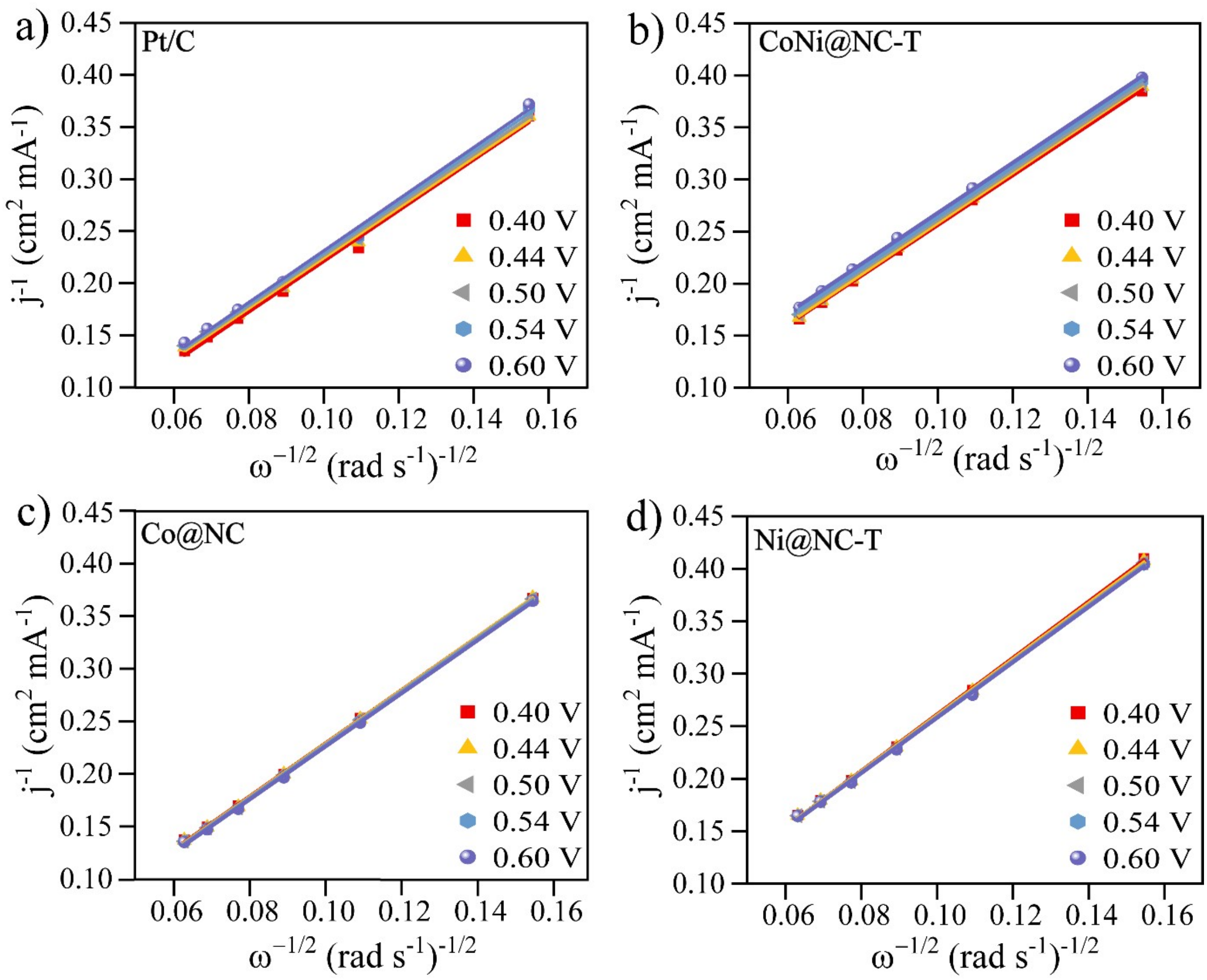

Fig. S15: (a-d) The Koutecky-Levich (K-L) plots derived from Fig. S14 at different potentials of 0.40 to 0.60 V for Pt/C, CoNi@NC-T, Co@NC and Ni@NC-T, respectively.

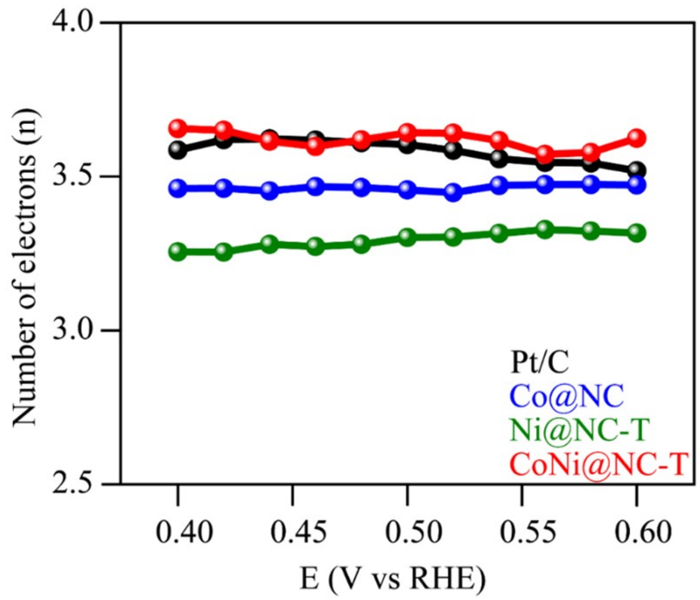

Fig. S16: Number of electrons derived from the Koutecky-Levich (K-L) equation derived from Fig. S15 at different potentials of 0.40 to 0.60 V for Pt/C, CoNi@NC-T, Co@NC and Ni@NC-T, respectively.

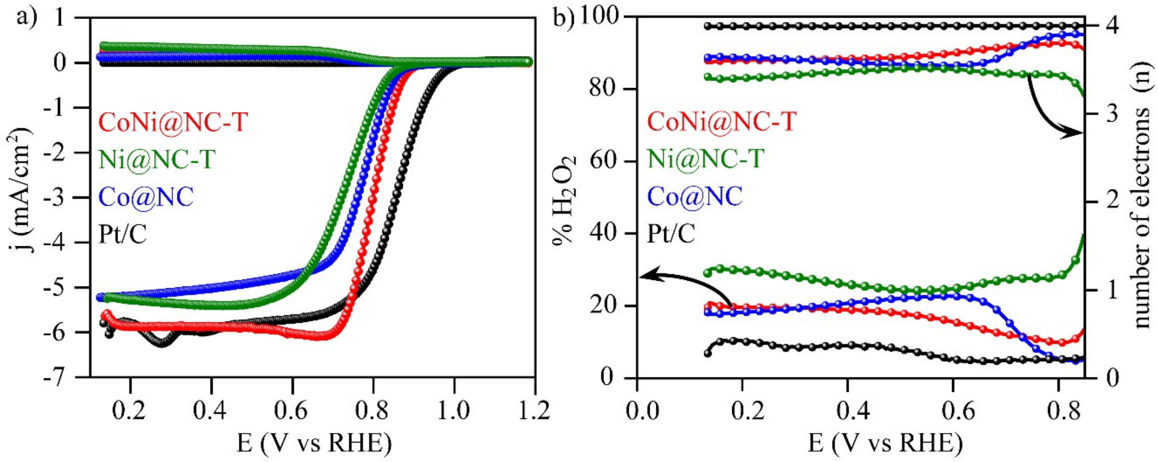

Fig. S17: RRDE study for Pt/C, CoNi@NC-T, Co@NC and Ni@NC-T. (a) RRDE curves recorded for ORR and (b) change in number of electrons (n), and % of H_2O_2 with respect to the disk potential. Conditions: 1600 RPM, 5 mV/s scan rate, Electrolyte: oxygen saturated 0.1 M KOH solution.

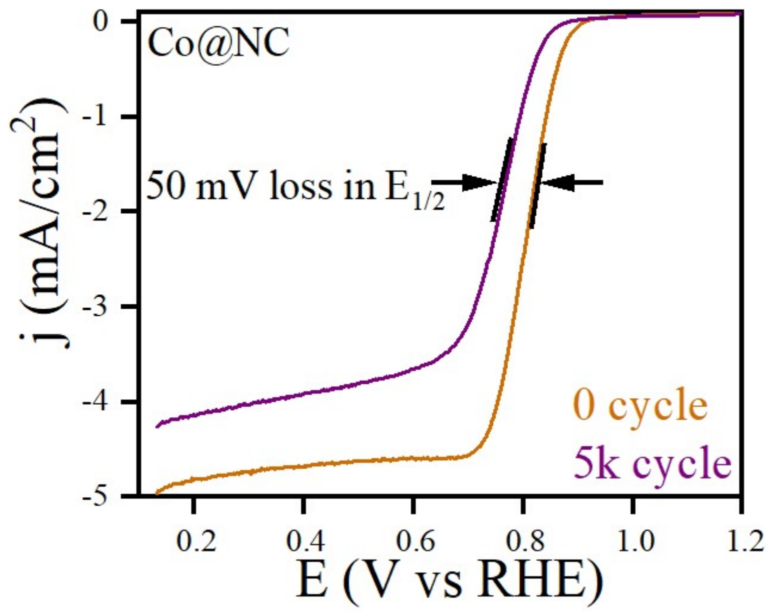

Fig. S18: ORR Stability LSV curves for Co@NC at before and after 5K potential cycles in O_2-saturated 0.1 M KOH. Conditions: 1600 RPM, 5 mV/s scan rate, Electrolyte: oxygen saturated 0.1 M KOH solution.

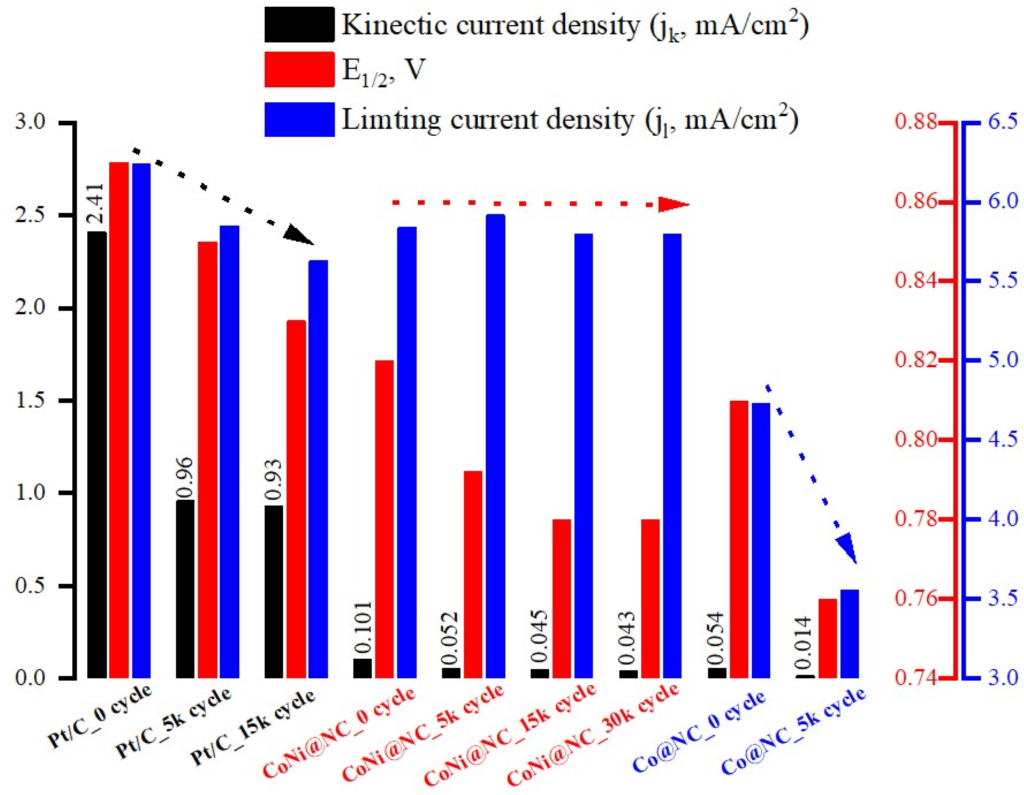

Fig. S19: Comparative bar graph indicates the change in $E_{1/2}$, j_k and j_l before and after cycling stability test for Pt/C, CoNi@NC-T and Co@NC.

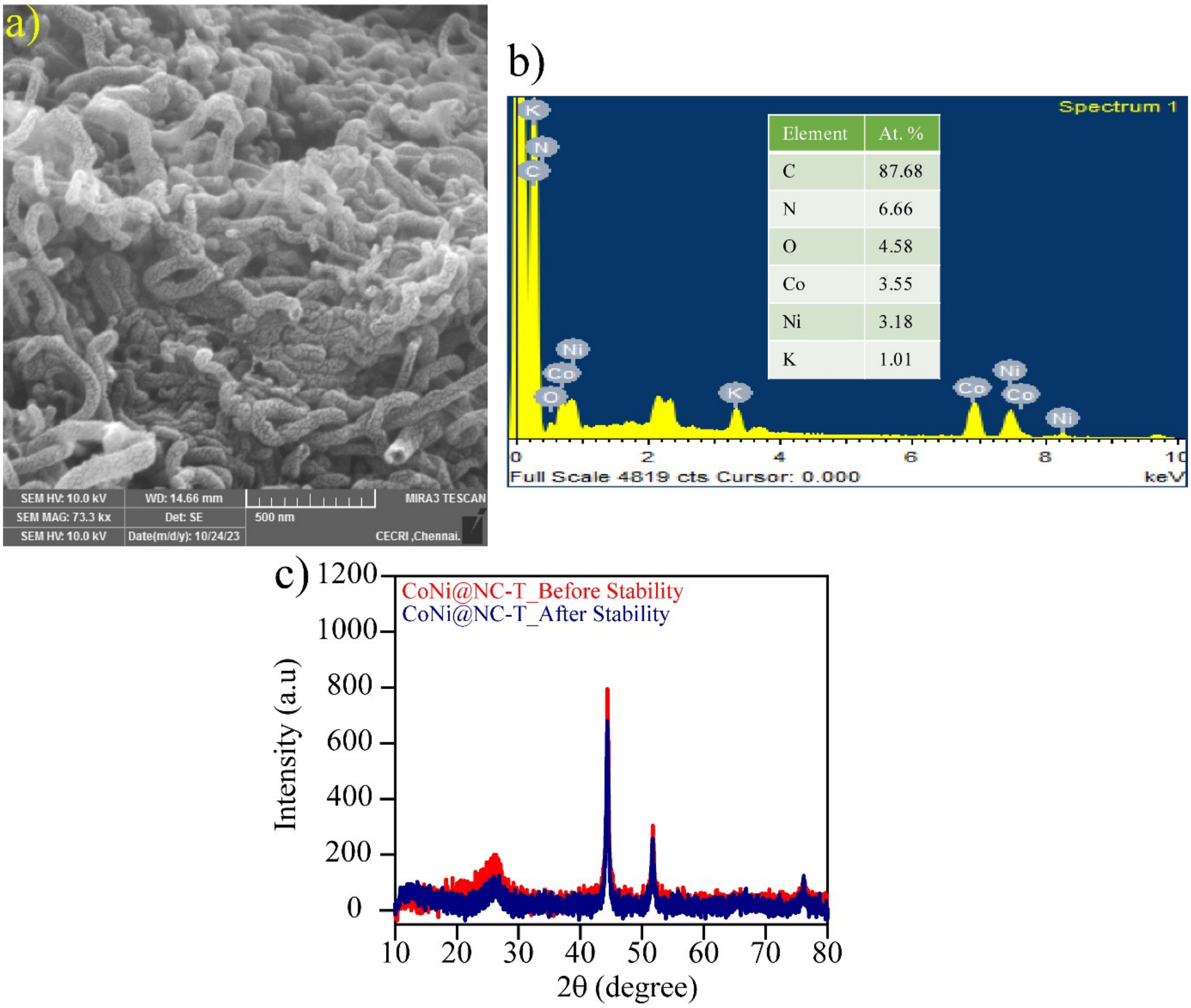

Fig. S20: Post 30000 cycles stability of CoNi@NC-T (a-b) Fe-SEM micrograph confirms the retention of tubular morphology and EDAX spectrum. In EDAX mapping a trace amounts of potassium concentration were observed on the tube's surface and are attributed to cation species adsorption from 0.1M KOH electrolyte. (c) Comparison of p-XRD patterns before and after the stability test.

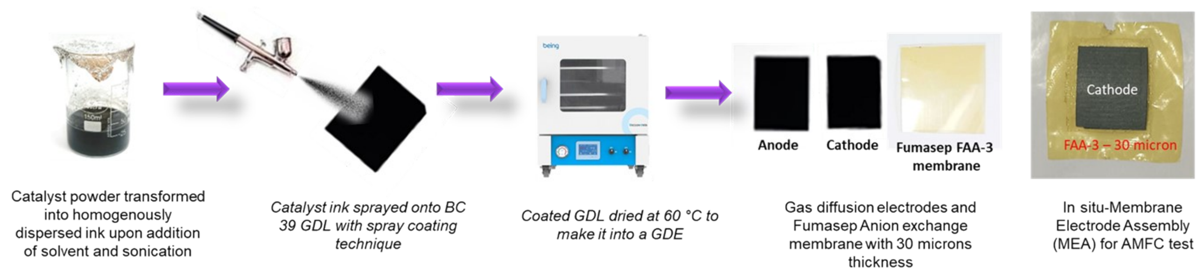

Fig. S21: Schematic procedure of electrode fabrication and membrane electrode assembly (MEA) for Anion Exchange Membrane Fuel Cell (AEMFC) application.

Table S3: Literature reports on Half-cell Stability and ORR LSV performance of non-precious electrocatalysts in 0.1 M KOH electrolyte.

S.No.	**Catalyst name**	**catalyst loading (mg/cm^2)**	**E_{onset} (V vs RHE)**	**$E_{1/2}$ (V vs RHE)**	**No of cycles**	**$\Delta E_{1/2}$ (mV vs RHE)**	**Reference No**
1.	**CoNi@NC-T**	**0.22**	**0.94**	**0.83**	**30000**	**18**	**This work**
2.	**Co@NC**	**0.22**	**0.93**	**0.82**	**5000**	**50**	**This work**
3.	**HiSPEC™ 4000 Pt/C**	**0.22**	**1.03**	**0.89**	**15000**	**33.3**	**This work**
4.	**Ni@NC-T**	**0.22**	**0.90**	**0.75**	**--**	**--**	**This work**
5.	Co/S/N-800	--	0.912	0.831	5000	5	*ChemSusChem* 2019,**12**,3390 – 3400.
6.	Co/NGC-3	0.20	0.94	0.85	8000	12	*ACS Appl. Mater. Interfaces,* 2020, **12(5)**, 5717–5729.
7.	NFC@Fe/Fe_3C-9	0.6	0.991	0.87	50000	26	*Nanoscale*, 2020,**12**, 2542-2554.
8.	CNF@Zn/CoNC	0.25	0.91	0.82	1000	No change	*Small*, 2018, **14**, 1704207.
9.	NiCoOS	--	0.88	0.79	800	Negligible loss	*Nano energy*, 2019, **58**, 680-686.
10.	$NiCo_2S_4$@g-C_3N_4-CNT	0.12	0.87	0.76	6000	Negligible loss	*Adv.Mater.*, 2019, **31**, 1808281.
11.	FeCo-NCNFs-800	0.255	0.907	0.817	--	--	*ACS Sustainable Chem. Eng.,* 2019, **7(5)**, 5462–5475.
12.	FeCo-NSCNF@NCNT	0.3	0.85	0.792	--	--	*J. Power Sources*, 2019, **421**, 68-75.
13.	FCx-NC/CNTs-10	0.256	0.90	0.76	--	--	*J. Power Sources*, 2019, **438**, 227019.
14.	Co_3O_4/NPGC	0.2	0.97	0.85	--	--	*Angew. Chem. Int. Ed.*, 2016, **55**, 4977 – 4982.
15.	Co_3S_4@N, S-rGO	0.28	0.91	0.76	--	--	*ACS Appl. Mater. Interfaces*., 2013, **5**, 5002.
16.	Co/N-BCNTs	0.20	--	0.83	--	--	*J. Mater. Chem. A, 2018, **6**, 5752-5761.*
17.	Co@Co_3O_4/NC-1	0.21	0.93	0.74	--	--	Angew.Chem.Int. Ed., 2016, **55**, 4087–4091.
18.	Co-Fe/NC-700	0.25	--	0.85	--	--	*Small*, 2019, **15**, 1805324.
19.	Co_3O_4@Co/NCNT	--	0.9	--	--	--	*Inorg. Chem.*, 2020, **59(5)**, 3160–3170.
20.	$Co_{0.5}Fe_{0.5}S$@N-MC	0.8	0.91	0.82	--	--	*ACS Appl. Mater. Interfaces,* 2015, **7(2)**, 1207–1218.

21.	S-600	0.3	0.95	0.84	2000	No change	*Nanoscale*, 2018**,** **10**, 21076-21086.
22.	CoZn/NC	0.4	0.919	0.852	5000	15	*J. Alloys Compd.*, 2024, **983**, 173878.
23	Fe-Sn-N/C	--	1.1	0.92	10000	37	Small Methods, 2024, 2301674 (Early View)
24.	Fe-N/P-C-700	0.6	0.94	0.86	--	--	*J. Am. Chem. Soc.*, 2020, **142**, 2404-2412.
24	CoNi/N-C-800	--	0.91	0.81	1000	Negligible loss	*Int. J. Hydrogen Energy*, 2023, **48(69)**, 26979-26989.
25.	CoNi@N-GCNT-FD	--	0.90	0.84	10000	Negligible loss	*ACS Sustainable Chem. Eng.,* 2021, **9(24)**, 8207–8213.

Table S4: Reported anion exchange membrane fuel cell (AEMFC) performance of various type of membrane.

S.No.	Membrane-type and thickness (microns)	Anode loading (mg/cm^2)	Cathode loading (mg/cm^2)	Temp. (°C)	Peak power density (mW/cm^2)	Reference
1.	GT82-15/PTFE	PtRu_0.7	Pt/C_0.6	85	3370	*Journal of The Electrochemical Society*, 2019, **166**, F637-F644.
2.	PFTP-13 (20 µ)	PtRu_0.42	Pt/C_0.33	80	2050 to 2340 (with BP)	*Nat Commun*, 2021,**12**, 2367.
3.	TPN (30 µ)	PtRu_0.5	Pt/C_0.6	85	1450 (with BP)	*Energy Environ. Sci.,* 2018,**11**, 3283-3291.
4.	BTMA-HDPE	PtRu_0.4	Pt/C_0.4	80	2550	*Energy Environ. Sci.,* 2019, **12**, 1575-1579.
5.	BTMA-LDPE	PtRu_0.4	Pt/C_0.4	80	2010	
6.	F20C9N	PtRu_0.7	Pt/C_0.5	60	1010	*Adv. Funct. Mater.,* 2019, **29(26)**, 1902059.
7.	Recast-FAA3	Pt/C_0.3	Pt/C_0.3	60	90.6	*ACS Appl. Energy Mater.,* 2023, **6(24)** 12549–12559.
8.	FAA-3-50 (50 µ)	BASF Pt/C_0.8		60	223	*J. Power Sources*, 2013, **230**, 169-175.
9.	A201 Tokuyama® Membrane (28 µ)	Tanaka Pt/C_0.4	Tanaka Pt/C_0.6	45	120	*Int. J. Hydrogen Energy*, 2012, **37**, 4406-4412.
10.		E-TEK_0.4	E-TEK_0.6	45	~100	
11.	FAA-3-50 (50 µ)	Pt/C_0.5		RT	68	*J. Power Sources*, 2017, **353**, 104-114.
12.	FAA-3-50	Pt/C_0.5	MoS_2/G-500	RT	29	

	(50 µ)					
13.	T20NC6NC5N	Pt/C_0.5		60	105 (with BP)	*Macromolecules*, 2016, **49(3)**, 815–824.
14.	D30NC6NC6				260 (with BP)	
15.	S60NC6				364 (with BP)	
16.	TPQPOH15	Pt/C_0.2		70	258 (with BP)	*ChemSusChem*, 2010, **3(5)**, 555-558.
17.	A201 Tokuyama® Membrane (28 µ)	Pt_0.4	CoFe/NC_4	50	177	*J. Power Sources*, 2011, **196**, 1717–1722.
18.		Pt_0.4	Pt/C_0.4	50	196	
19.	HMT-PMBI	TKK PtRu/C_0.8	Pt/C_0.4	60	350 (with BP)	*Electrochim. Acta*, 2020, **334**, 135575.
20.		TKK PtRu/C_0.8	Pyr.KB/FePc_2	60	186 (with BP)	
21.	aQAPS-S8 (40 µ)	PtRu/C_0.4	MCS(Mn-Co) _ 0.58	60	1100 (with BP)	*Nat Commun*, 2019, **10**, 1506.
22.	A201 membrane (Tokuyama) (28 µ)	TKK Pt/C_0.4	TKK PT/C_0.4	60	479	*Energy Environ. Sci.*, 2019, **12**, 2200-2211.
23.		TKK Pt/C_0.4	40 wt% Co@G/C_600_0.4	60	412	

Table S5: Reported anion exchange membrane fuel cell (AEMFC) performance with fumion based membrane with different thickness FAA-3-*x*, *x*=20-, 30-, 50- and 130-micron thickness.

S.No.	Membrane thickness	Anode loading (mg/cm²)	Cathode loading (mg/cm²)	Temp. (°C)	Peak power density (mW/cm²)	Reference
1.	**30**	**HiSPEC™ 4000 Pt/C_ 0.7**	**CoNi@NC-T_1.5**	**30**	**170**	**This work**
2.	**30**	**HiSPEC™ 4000 Pt/C_ 0.7**	**CoNi@NC-T_1.0**	**30**	**157**	**This work**
3.	**30**	**HiSPEC™ 4000 Pt/C_ 0.7**	**CoNi@NC-T_0.7**	**30**	**128**	**This work**
4.	**30**	**HiSPEC™ 4000 Pt/C_ 0.7**	**HiSPEC™ 4000 Pt/C_0.7**	**30**	**153**	**This work**
5.	50	Pt/C_0.8	Pt/C_0.8	60	175	*J. Power Sources*, 2015, **277**, 147-154.
6.	50	Pt/C_0.8	Co-Fe_3O_4/C_0.8	60	114	
7.	20	TKK Pt/C_0.33	TKK Pt/C_0.33	65	300 to 500 (with BP)	*Nat Commun,* 2021, **12**, 2367.
8.	50	TKK Pt/C_0.33	TKK Pt/C_0.33	65	300 to 400 (with BP)	
9.	130	E-TEK Pt/C_0.5	E-TEK_0.5	50	62	*J. Phys. Chem. C,* 2012, **116(6)**, 4340–4346.
10.	130	E-TEK Pt/C _0.5	N-CNT_5	50	38	
11.	Unknown	Pt/C_0.4	Co/NC_4	60	271	*Appl. Catal. B*, 2020, **260**,118192.
12.	50	Pt/C_0.8	Co-NC-900_2	50	60	*ChemElectroChem*, 2017, **4(11)**, 2928-2933.
13.	50	E-TEK Pt/C_0.8	NpGr-72_2.5	50	27	*Energy Environ. Sci.*, 2014, **7**, 1059-1067.
14.	50	Pt/C_0.5	Fe/N–F/CC-C_0.5	45	38	*Energy Fuels,* 2022, **36(4)**, 2108–2122.

15.	50	Pt/C_0.5	$Ni_{20}Co_{20}$@B/GNF-H_0.5	45	70	*ACS Appl. Energy Mater.,* 2022, **5(8)**, 10240–10253.
16.	50	Pt/C_0.5	Pt/C_0.5	45	85	
17.	50	Pt/C_0.12	NiCo/NCNT (1:1) _4	50	65	*Renew. Energy,* 2020, **154**, 508-516.
18.	50	Pt/C_0.5	N–F/PGPC_2	35	22	*Sustainable Energy Fuels***,** 2021**, 5**, 886-899.
19.	50	Pt/C_0.5	N-GLC_1.5	25	6	*Bull Mater Sci,* 2021, **44**, 135.
20.	50	Pt/C_0.5	Pt/C_0.5	60	140	*ChemElectroChem, 2022,* ***10(3)****, e202201052.*
21.	Unknown	Pt/C_0.2	Pt/C_0.2	60	74	*Int. J. Hydrogen Energy,* 2024, **52©**, 139-153.
22.	50	Pt/C_0.2	Pt/C_0.2	60	91.6	*ACS Appl. Energy Mater.,* 2023, **6(14)**, 7702–7713.
23.	50	Pt/C_0.5	Fe-N-C-1000_4.5	60	149	*Chem. Eng. J.*, 2023, **465**, 142987.
24.	Unknown	Pt/C_0.35	Fe-Fe_2O_3/NGr_3.0	60	54	*Nanoscale*, 2015, **7**, 20117–20125.
25.	50	Pt/C_0.5	1.3 Fe	60	87	*ChemElectroChem*, 2023, **10**, e202201115.